

## Influence of Particle Elongation and Aspect Ratio on the Discharge Behavior of a Flat-Bottom Silo<sup>†</sup>

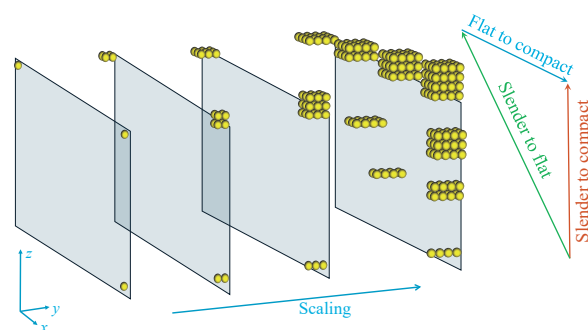
Yani Alhaddad<sup>1</sup> and Álvaro Ramírez-Gómez<sup>1,2\*</sup>

<sup>1</sup> Department of Mechanical, Chemical, and Industrial Design Engineering, Universidad Politécnica de Madrid, Spain

<sup>2</sup> Safety and Quality in Energy and Mining Industries Technology Centre (TECMINERGY), Spain

Silos are widely used structures designed with hoppers or as flat bottoms to store different types of particulate materials (pellets, grains, powders, etc.). Although they have been used in industry for a long time, further research is needed. This article provides design recommendations that prevent structural failures and ensure efficient discharge. The discrete element method (DEM) has been commonly used in recent decades in silo/bin research to simulate the behavior of stored materials. In this study, DEM was used to investigate the relationship between the slot width and particle size on the discharge behavior in a flat-bottom silo using particle shape configurations with different elongations and aspect ratios. Sixteen DEM models were developed using the multi-sphere approach to obtain the particle configurations, ranging from single spheres to  $4 \times 4 \times 4$  clusters of spheres arranged along orthogonal axes ( $x$ ,  $y$ , and  $z$ ). The simulations involved between 459 and 29,383 particles with a total mass of 40 kg in each model. The established comparisons include information on the bulk density, velocity profiles, residual masses, and discharge rates.

**Keywords:** discrete element method (DEM), particle shape, multi-sphere, flat-bottom silo, discharge, elongation, aspect ratio



### 1. Introduction

Solids handling is essential in various sectors, such as agriculture, energy, and mining. Advances in solids handling have enabled solutions for transporting, conveying, and storing solids safely and efficiently (Gelmar and Zegzulka, 2019). Among storage solutions, silos are structures designed to store bulk materials while protecting them from quality degradation and environmental factors. Understanding particle interactions within silos is crucial for predicting flow patterns during discharge, which helps to prevent flow-related issues, such as clogging, arching, and inconsistent or unsteady flow (Alonso-Marroquín et al., 2013).

The discrete element method (DEM), introduced by Cundall and Strack (1979), is a numerical technique that simulates particle interactions and predicts their behavior. DEM is capable of effectively modeling a wide range of phenomena in granular materials, whether densely or loosely packed, stationary, or in motion, under rapid or slow conditions (Horabik et al., 2022; Ramírez et al., 2010;

Ramírez-Gómez et al., 2020; Žurovec et al., 2019). However, challenges remain in using DEM, such as how to face the high computational cost of simulating a large number of particles and the influence of particle shape on simulations (Radvilaitė et al., 2016). While incorporating realistic particle shapes into simulations can yield predictions closer to real-life behavior, this often comes at the expense of increased computational demands. Therefore, simplifying particle shape representations has been a common practice in DEM since its inception, despite their impact on simulation accuracy. One simplification technique involves representing particles as clusters of spheres (Favier et al., 1999).

Among the different types of silos, the flat-bottom is one of the most common and cost-effective storage solutions, and it is characterized by flat-ground supports (Fig. 1). These silos allow the optimization of space utilization using different geometric configurations. The dimensions of the discharge openings are critical and must be carefully designed to ensure a smooth discharge and minimize stagnant zones, where material accumulation can occur. The design of the openings, the type of stored materials, and the location of the discharge openings in the silo influence the discharge rates.

Several studies have experimentally investigated the relationship between the size of the outlet and the flow of particles in flat-bottom silos, providing different recommendations. Langmaid and Rose (1957) explored various

<sup>†</sup> Received 31 May 2024; Accepted 8 November 2024  
J-STAGE Advance published online 25 March 2025

\* Corresponding author: Álvaro Ramírez-Gómez;

<sup>1</sup> Add: Ronda de Valencia, 3, Madrid, Spain

<sup>2</sup> Add: Tecnogetafe; Calle Eric Kandel, 1; 28906 Getafe, Madrid, Spain  
E-mail: alvaro.ramirez@upm.es  
TEL: +34-91-067-7637

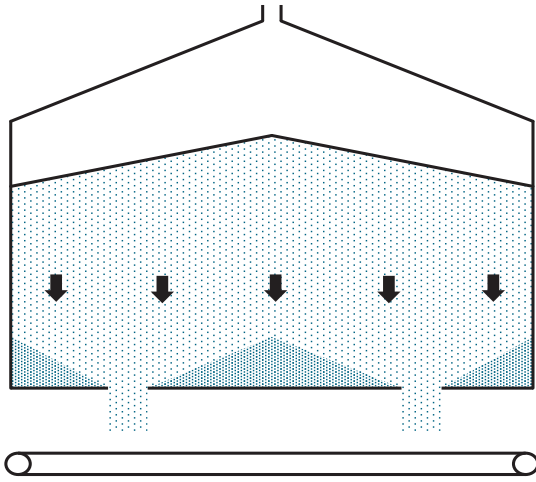


Fig. 1 Sketch of a flat-bottom silo and a horizontal conveyor.

particulate materials using a flat-bottom silo. They found that a  $K/P$  ratio of at least 5.36 is necessary to ensure smooth flow through a slit opening (rectangular and longer in one dimension) and of at least 4.32 for circular openings. Here,  $K$  is the perimeter diameter of the orifice, and  $P$  is the mean particle size. Brown and Richards (1965) also examined this relationship, reporting a  $K/P$  ratio between 6 and 9 for circular openings. Nedderman et al. (1982) suggested a critical threshold for the outlet width-to-particle diameter ratio in cylindrical flat-bottom silos with circular openings, indicating that discharge becomes intermittent if the outlet width is less than six times the particle size. The geometry of the outlet, as well as the size and shape of the particle, influences the determined  $K/P$  ratio. The research conducted to determine this ratio mainly used round particles such as glass beads. Further research on the determination of this ratio using different particle shapes (elongated, flat, or compact) is required.

The particle size can be easily determined in spherical or almost round particles by measuring the particle diameter. However, the particle size depends on the method used for this purpose when the particle shape is complex. Various techniques can be used to obtain the size of the particles: sieves, laser diffraction, and image analysis. The determination of the particle size when its shape is not round can be obtained in two dimensions (2D) by measuring specific dimensions such as the longest and shortest axis (Feret diameters) or the diagonal length. In three dimensions (3D), the size can be assessed by obtaining the diameter of the sphere with a volume equivalent to that of the particle or by measuring the diagonal length of the minimum bounding box (Fig. 2).

The DEM was used to examine the ratio between the outlet width of a flat-bottom silo and the particle size. Here, the equivalent diameter of the particle, Feret diameters ( $P_L$ ,  $P_S$ ), and diagonal lengths in 2D ( $P_{d2D}$ ) and 3D ( $P_{d3D}$ ) are

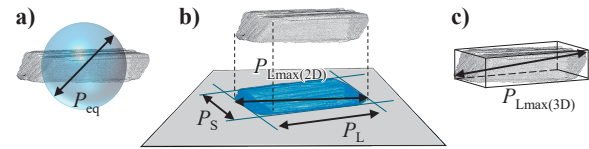


Fig. 2 Different dimensions considered for particle size determination: a) equivalent diameter, b) Feret diameters, and diagonal length in 2D, c) diagonal length in 3D.

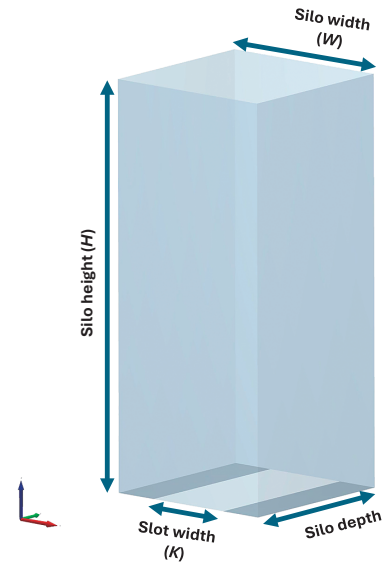


Fig. 3 Silo model.

considered. Particles with different elongations and aspect ratios were also used.

## 2. Methodology

### 2.1 Models and simulations

In this study, a flat-bottom silo of plexiglass with a square cross-section and a rectangular slot opening was used. The silo has a square cross-section of  $300 \times 300$  mm and a height of 700 mm. The outlet size, positioned centrally as shown in Fig. 3, is  $150 \text{ mm} \times 300 \text{ mm}$ .

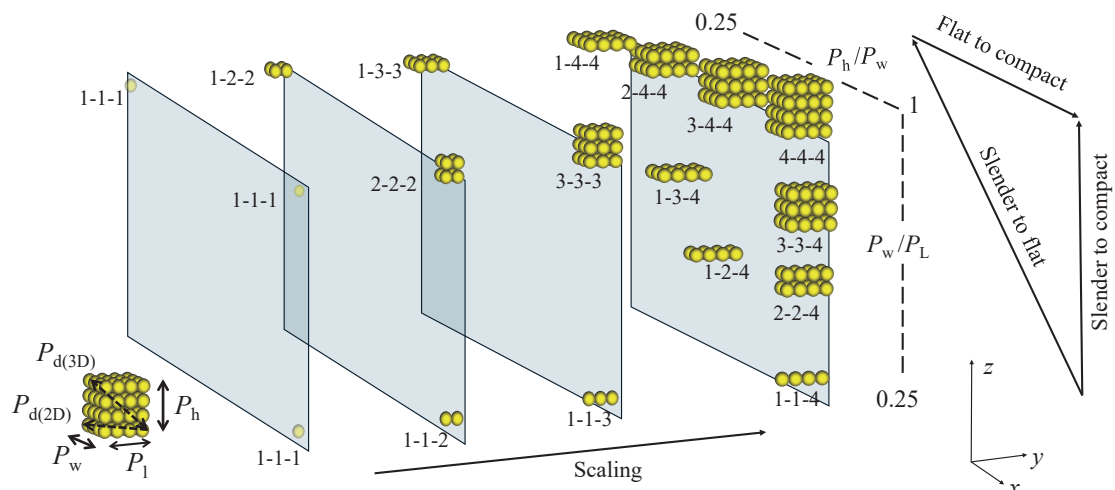
Sixteen particle shape configurations were analyzed, ranging from a single sphere with a diameter of 10 mm to a compact cubic cluster of spheres with a side length of 40 mm, as shown in the lower left corner of Fig. 4. Each particle configuration is labeled using the nomenclature  $x$ - $y$ - $z$ , where  $x$ ,  $y$ , and  $z$  indicate the number of spheres added in each orthogonal direction. For instance, the 4-4-4 configuration corresponds to a compact particle composed of 64 spheres (four spheres in each orthogonal axis). The principal dimensions of the particle— $P_l$  (length),  $P_w$  (width), and  $P_h$  (height)—used to generate the different particle shape configurations are also shown in Fig. 4, along with the diameter length in 2D ( $P_{d2D}$ ) and 3D ( $P_{d3D}$ ). By varying these principal dimensions, slender ( $P_l > P_w$ ), flat ( $P_h < P_w$ ), and compact particles ( $P_l = P_w = P_h$ ) were obtained. All particle shape configurations follow this

relation between these dimensions:  $P_1 \geq P_w \geq P_h$ . The elongation (EL) is defined as  $(\Delta P_1 + P_1)/P_1$ , and the aspect ratio (AR) is defined as the relation between the longest and shortest dimensions of the particle cross-section.

A total of six comparisons were conducted (**Table 1**). Comparisons #1, #2, and #3 focused on slender, flat, and compact particles, respectively, with their sizes increased and using a model with spherical particles as a reference. Comparison #4 examined the transition from slender to compact shapes, while comparison #5 explored the transition from slender to flat shapes and comparison #6 explored

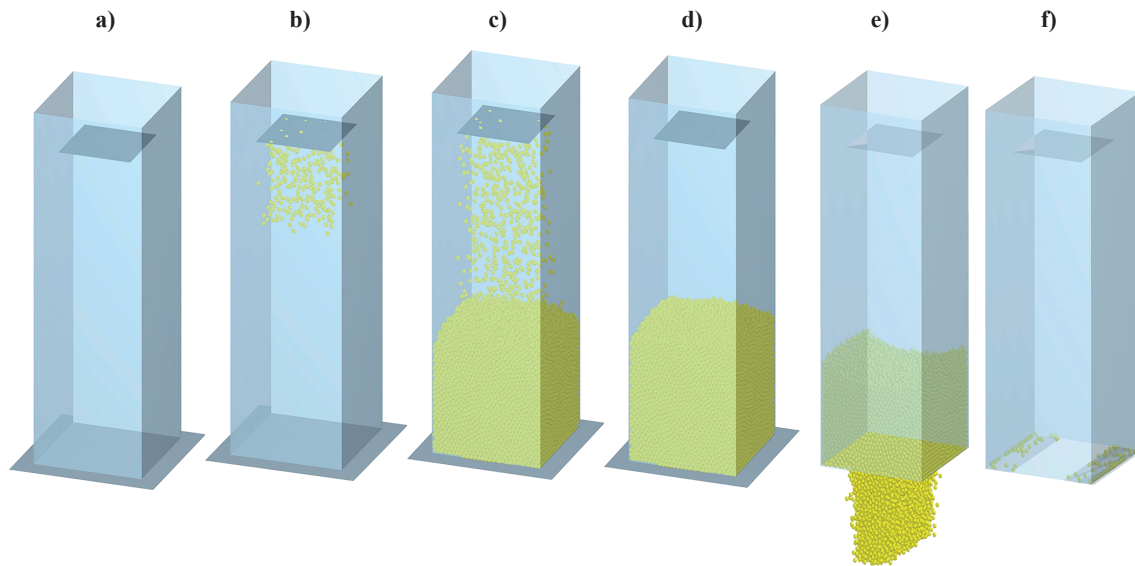
the transition from flat to compact shapes.

All simulations were performed using the Professional Edition of EDEM 2022.3 (EDEM, 2023). Using the Euler integration, the Rayleigh percentage was set at 20 %, and the time step was  $1.12 \times 10^{-6}$  s. The filling process involved the progressive generation of particles using a square virtual surface measuring  $200 \times 200$  mm, positioned at the center of the silo and 600 mm above the base. The number of particles in the simulations ranged from 459 to 29,383, with a total mass of 40 kg in each case. After the filling process and 4–6 seconds after the material



**Fig. 4** Particle shape configurations.

**Table 1** Comparisons of different particle shape configurations (in red color).



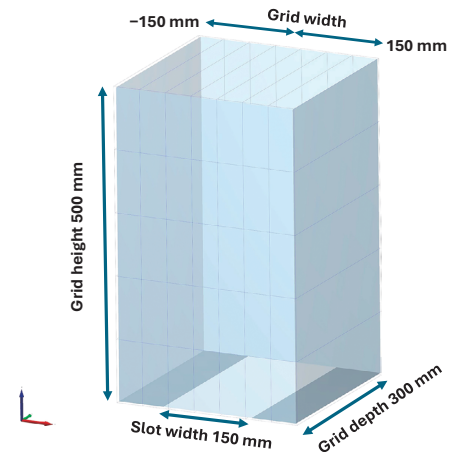
**Fig. 5** Filling and discharge processes using a virtual surface: **a)** silo before filling, **b)** initial stage of the filling process, **c)** filling process, **d)** static equilibrium, **e)** discharge process, **f)** silo after discharge.

inside the silo reached static equilibrium, the outlet was opened to initiate discharge. The discharge process was considered complete when the silo was empty. **Fig. 5** provides a step-by-step illustration of the filling and discharge processes.

To provide information on the models developed to examine the  $K/P$  ratio, bulk density, velocity profiles, residual masses, and discharge rates were obtained.

The distribution of the bulk density  $\rho_b$  indicates the influence of particle shape and size on the packing behavior. This parameter was obtained in all models once the silo was filled and the particles had reached complete static equilibrium. The procedure followed involved dividing the volume inside the silo into grid cells. A total of 35 grid cells were considered, each with dimensions of  $42.85 \text{ mm} \times 300 \text{ mm} \times 100 \text{ mm}$  (**Fig. 6**). The total bulk density (TBD) was obtained by considering the overall volume of the stored material in the silo.

Velocity profiles were recorded at two instants of time (0.1 s and 0.2 s) and at five heights above the outlet: 50, 150, 250, 350, and 450 mm. These velocity profiles were obtained by averaging the velocities of the particles within each of the seven cells at the specified heights. The residual masses and discharge rates were obtained to identify the presence of fluctuations during discharge. The residual mass represents the mass remaining in the silo after the outlet opening. Two types of discharge rates were determined: the overall discharge rate ( $DR_L$ ) and the instantaneous discharge rate ( $DR_I$ ).  $DR_L$  was obtained as the ratio of the total discharge mass to the time interval corresponding to the linear region ( $DT_L$ ) in the residual mass vs. time plots.  $DR_I$  was obtained over a simulation time interval of 0.04 s to capture variations in discharge rates. The average was calculated in the instantaneous discharge rate plots



**Fig. 6** Silo volume divided into 35 grid cells, each measuring  $42.85 \text{ mm} \times 300 \text{ mm} \times 100 \text{ mm}$ .

during the peak zone using a dashed line. This parameter was used to determine standard deviations to obtain information on the fluctuations that occurred during discharge.

The material properties of the silo walls (plexiglass) and spheres (glass beads) are listed in **Table 2**. These properties were obtained from a previous study (Bharadwaj et al., 2010). **Table 3** presents the interaction parameters used in the discrete element simulation to model the interaction between the glass beads and silo walls.

### 3. Results and discussion

The results obtained from the six established comparisons and the determined  $K/P$  ratios are presented and discussed below.

#### 3.1 Comparison #1

Four models were considered, each using particles with



**Table 2** Material properties used in DEM simulations.

Property	Wall	Particles
Density (kg m <sup>-3</sup> )	2500	2600
Shear modulus (Pa)	$24 \times 10^9$	$24 \times 10^9$
Poisson's ratio	0.3	0.25

**Table 3** Contact interactions.

Property	Particle-to-Wall	Particle-to-Particle
Coeff. of restitution	0.85	0.6
Coeff. of friction	0.1	0.1

different elongations (EL = 2, 3, and 4) and an identical aspect ratio of the cross-section ( $P_h/P_w$ ). **Fig. 7** illustrates the total bulk density (TBD) and the bulk density distribution in each model. In this figure, the color gradient ranges from red (indicating the highest density) to dark blue (indicating the absence of particles in that region).

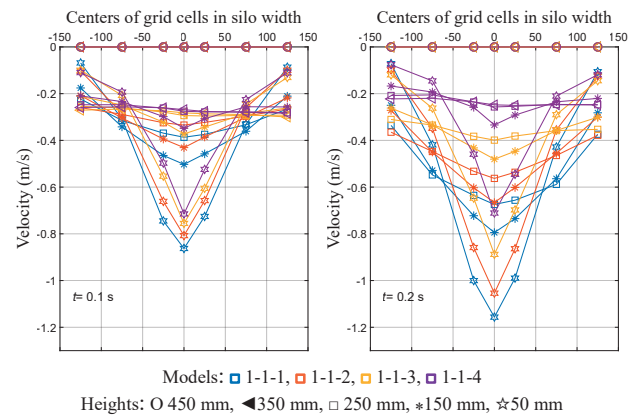
The total bulk density for the models with particle elongations of EL = 2, 3, and 4 was 5 %, 14 %, and 23 % lower, respectively, than that of the model with spherical particles, which achieved more efficient packing.

When comparing the models with elongated particles, we observed that the variation in bulk density was not proportional to the degree of elongation. In terms of bulk density distribution, the central region of the silo in all three models showed a red color with similar tones of red, indicating denser packing in that area. The vertical bands of lighter red near the silo walls indicate lower densities.

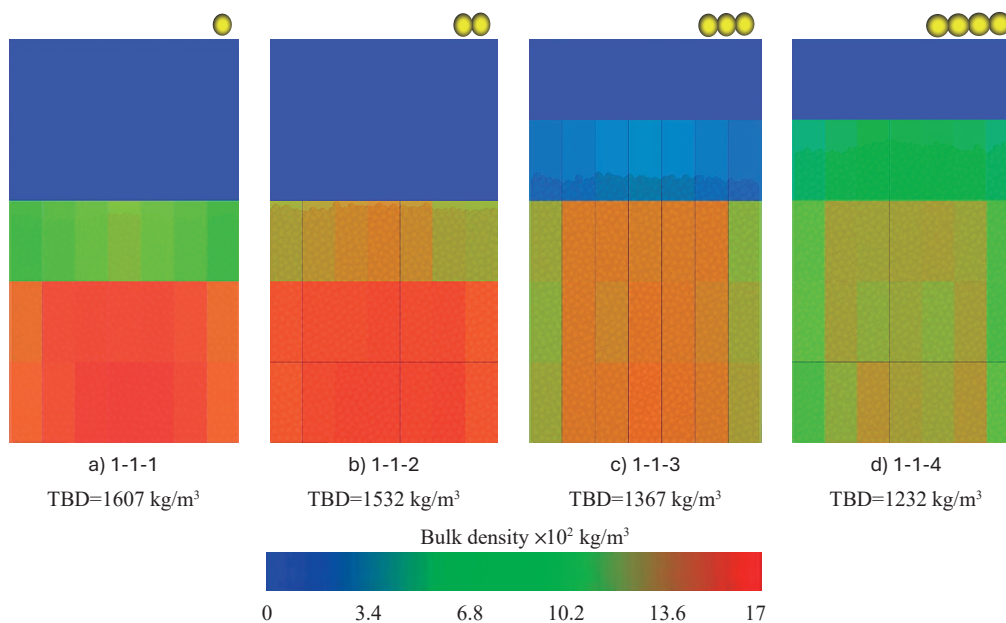
This can be attributed to the filling method, which involved centered and progressive filling, causing particles to

slide and roll from the center toward the walls as they accumulate. **González-Montellano et al. (2012)** observed a similar phenomenon using a comparable filling method in a silo with a pyramidal hopper.

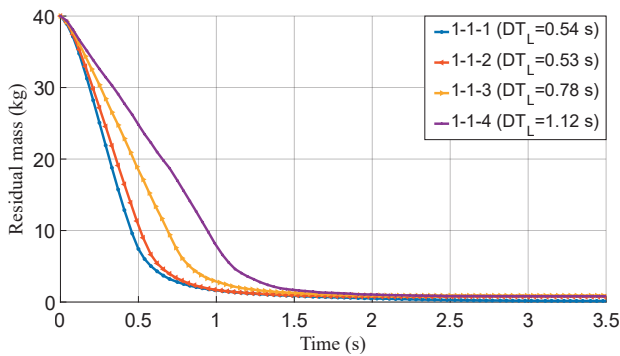
**Fig. 8** shows the velocity profiles, which exhibit a V-shape below a height of 250 mm. The highest velocity values were observed for spherical particles. At a height of 50 mm, the velocities at 0.1 s were 0.86, 0.80, 0.75, and 0.71 m/s, while at 0.2 s, they were 1.15, 1.05, 0.88, and 0.71 m/s for all models. A 38 % difference was observed at  $t = 0.2$  s when comparing the model with the most elongated particles (EL = 4) to the model with spherical particles, highlighting the geometric interlocking effect produced during discharge. The rotation of non-spherical particles partially hindered their movement toward the outlet.



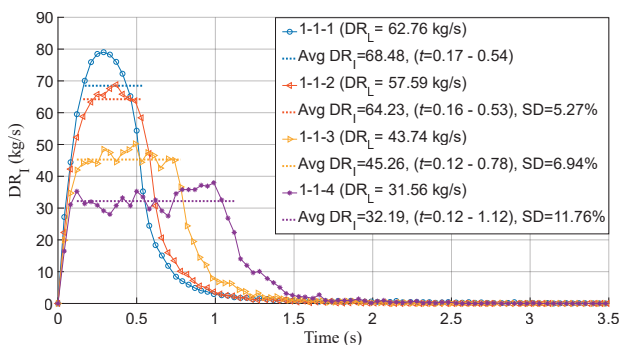
**Fig. 8** Velocity profiles of the considered models obtained during discharge at different heights from the outlet, ranging from 50 mm to 450 mm, and at two instants of time,  $t = 0.1$  s and  $t = 0.2$  s, comparison #1. The raw data are publicly available at J-STAGE Data (<https://doi.org/10.50931/data.kona.28561904>).



**Fig. 7** Distribution of density in the silo and total bulk density (TBD) in the models of comparison 1: a) 1-1-1, b) 1-1-2, c) 1-1-3, d) 1-1-4.



**Fig. 9** Residual mass in the silo (kg) vs. discharge time (s), elongation variation. The raw data are publicly available at J-STAGE Data (<https://doi.org/10.50931/data.kona.28561904>).



**Fig. 10** Instantaneous discharge rate ( $DR_I$ ) (kg/s) vs. time with 0.04 s time step, average instantaneous discharge rate (Avg  $DR_I$ ) (kg/s), and overall discharge rate values ( $DR_L$ ), elongation variation.

**Fig. 9** shows that models 1-1-1 and 1-1-2 exhibit similar behavior with respect to the residual mass of the stored material over time. This similarity is also reflected in **Fig. 10**, which presents the variation in the discharge rate over time. In the first two models (1-1-1 and 1-1-2), the material flowed smoothly, with only minor fluctuations detected in model 1-1-2, which occurred above the average value of the instantaneous discharge rate (Avg  $DR_I$ ). However, starting from model 1-1-3, the flow became increasingly erratic, with fluctuations of the instantaneous discharge rate values above and below Avg  $DR_I$ , and a standard deviation of these values (SD ( $DR_I$ )) of 6.94 % (**Table 4**). The most pronounced erratic behavior was observed in model 1-1-4 with SD ( $DR_I$ ) = 11.76 %.

### 3.2 Comparison #2

This comparison examines the effect of varying the size of flat particles with particle lengths and widths of 20, 30, and 40 mm while maintaining ( $P_h$ ) equal to 10 mm in all models. **Fig. 11** shows the bulk densities of models 1-1-1, 1-2-2, 1-3-3, and 1-4-4. A significant decrease in total bulk density was observed as particle size increased. More efficient packing is achieved with the smallest particles, whereas the largest particles present more voids; however, when falling in the silo, they tend to lie horizontally. The

total bulk density for models with  $P_h/P_w = 0.5$ , 0.33, and 0.25 was 15 %, 29 %, and 40 % lower, respectively, than the total bulk density of model 1-1-1 with spherical particles.

In **Fig. 12**, at a height of 50 mm, the velocities at 0.1 and 0.2 s varied significantly between models 1-1-1 and 1-4-4, indicating the influence of particle size on the flow dynamics. Larger particles have their movement significantly hindered, while particles in models 1-2-2 and 1-3-3 exhibited a more similar behavior, particularly when observing peak velocities at 0.1 s and 0.2 s. After these time points, the behavior of the discharge in these two models differs, as observed in **Figs. 13** and **14**. These figures show that the residual mass and instantaneous discharge rates differ significantly among the models. With the exception of models 1-1-1 and 1-1-2, if non-smooth flow is considered to occur when fluctuations of  $DR_I$  are over and below the average value (Avg  $DR_I$ ), irregular flow was observed in all other models. The most pronounced irregularities occurred in model 1-4-4.

As shown in **Table 4**, increasing the particle size by factors of 2, 3, and 4 resulted in discharge rates that were 25 %, 53 %, and 67 % lower, respectively.

### 3.3 Comparison #3







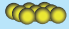
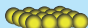




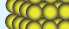
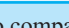


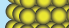


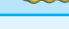
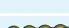

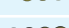

In comparison 3, models 1-1-1, 2-2-2, 3-3-3, and 4-4-4 were analyzed. Cubic-shaped particles of different sizes were considered but with the same aspect ratio ( $P_h/P_w$  and  $P_w/P_l$ ) and varying values of  $P_{d(3D)}$ , where  $P_l = P_w = P_h$  in all models. This comparison specifically investigates the effects of varying the size of compact particles. As shown in **Fig. 15**, similar to the observations in comparison #2 for flat particles, larger particles exhibited a more evenly distributed bulk density. The total bulk density for models of  $P_l = 2$ , 3, and 4 was 29 %, 40 %, and 44 % lower than that of model 1-1-1.

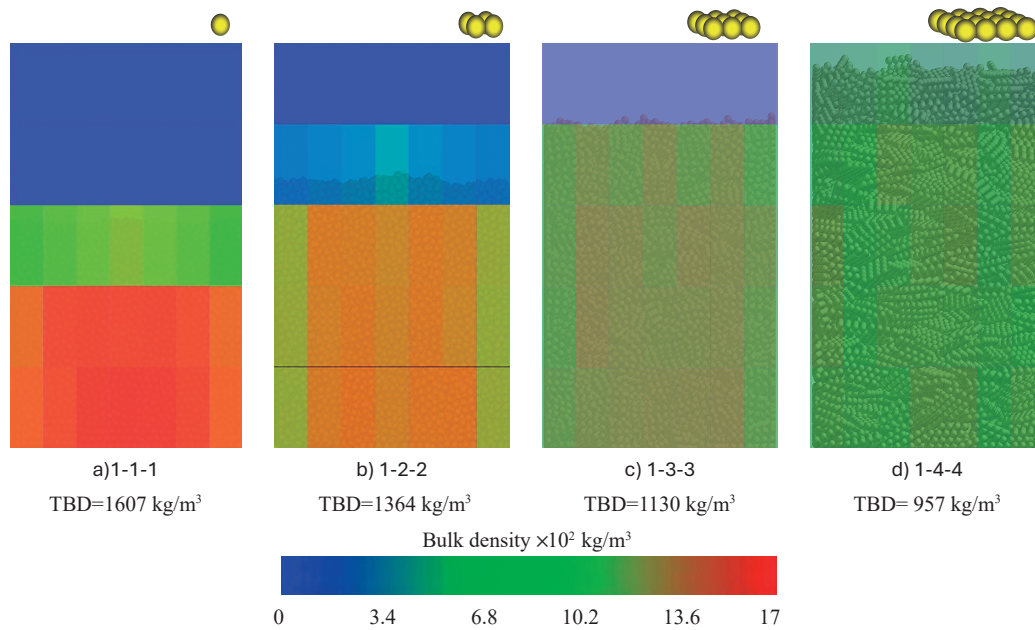
Small particles are packed more efficiently. Larger particles near the silo wall tended to be oriented with their face in contact with the wall. However, this does not occur inside the silo, resulting in more voids between them. **Fig. 16** shows the velocity profiles, which show a V-shape below 250 mm from the outlet.

At a height of 50 mm, the velocities at 0.1 and 0.2 s significantly varied among the models. This result highlights the influence of particle size on flow dynamics. The peak velocity at 0.1 s for the largest particles in model 4-4-4 was higher than that in model 3-3-3. Because of the size of the particles in model 4-4-4, the first particles are almost free-falling without impediment from others. However, in model 3-3-3, particles interlock from the initial instants of time.

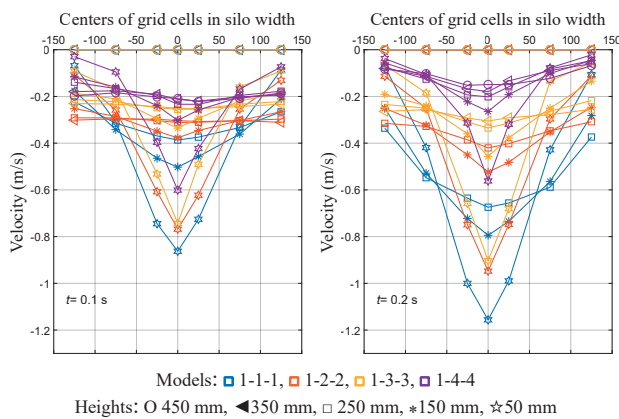
**Figs. 17** and **18** show that model 2-2-2 exhibits non-smooth behavior, with horizontal fluctuations observed in the velocity profiles.

**Table 4** Results obtained from all comparisons.

#	Model	EL	AR ( $P_b/P_w$ )/ ( $P_w/P_l$ )	TBD (kg m <sup>-3</sup> )	DR <sub>L</sub> (kg s <sup>-1</sup> )	DT <sub>L</sub> (s)	SD (DR <sub>l</sub> )	K/P <sub>eq</sub>	K/P <sub>l</sub>	K/P <sub>d(2D)</sub>	K/P <sub>d(3D)</sub>
1	Slender										
	1-1-1 	-	1/1	1607	62.76	0.54	Smooth	15	15	15	15
	1-1-2 	2	1/0.5	1532	57.59	0.53	5.27 %	11.90	7.5	7.5	7.5
	1-1-3 	3	1/0.33	1367	43.74	0.78	6.94 %	10.37	5	5	5
	1-1-4 	4	1/0.25	1232	31.56	1.12	11.76 %	9.44	3.75	3.75	3.75
2	Flat										
	1-1-1 	-	1/1	1607	62.76	0.54	Smooth	15	15	15	15
	1-2-2 	2	0.5/1	1364	46.94	0.7	6.89 %	9.44	7.5	6.25	6.25
	1-3-3 	3	0.33/1	1130	29.20	1.19	11.65 %	7.23	5	3.94	3.94
	1-4-4 	4	0.25/1	957	20.42	1.82	40.14 %	5.95	3.75	2.88	2.88
3	Compact										
	1-1-1 	-	1/1	1607	62.76	0.54	Smooth	15	15	15	15
	2-2-2 	2	1/1	1138	34.00	0.94	11.11 %	7.5	7.5	6.25	5.52
	3-3-3 	3	1/1	963	22.03	1.23	23.75 %	5	5	3.94	3.38
	4-4-4 	4	1/1	888	8.34	1.57	43.23 %	3.75	3.75	2.88	2.44
4	Slender to compact										
	1-1-4 	4	1/0.25	1232	31.56	1.12	11.76 %	9.44	3.75	3.75	3.75
	2-2-4 	4	1/0.5	1021	24.55	1.39	16.11 %	5.95	3.75	3.63	3.50
	3-3-4 	4	1/0.75	950	clog	0.3	35.75 %	4.54	3.75	2.88	2.95
	4-4-4 	4	1/1	888	8.34	1.57	43.23 %	3.75	3.75	2.88	2.44
5	Slender to flat										
	1-1-4 	4	1/0.25	1232	31.56	1.12	11.76 %	9.44	3.75	3.75	3.75
	1-2-4 	4	0.5/0.5	1111	28.17	1.23	12.47 %	7.5	3.75	3.63	3.63
	1-3-4 	4	0.33/0.75	1035	28.15	1.19	26.90 %	6.55	3.75	3.28	3.28
	1-4-4 	4	0.25/1	957	20.42	1.82	40.14 %	5.95	3.75	2.88	2.88
6	Flat to compact										
	1-4-4 	4	0.25/1	957	20.42	1.82	40.14 %	5.95	3.75	2.88	2.88
	2-4-4 	4	0.5/1	959	14.58	1.88	42.73 %	4.72	3.75	2.88	2.82
	3-4-4 	4	0.75/1	905	14.68	1.89	34.75 %	4.12	3.75	2.88	2.65
	4-4-4 	4	1/1	888	8.34	1.57	43.23 %	3.75	3.75	2.88	2.44



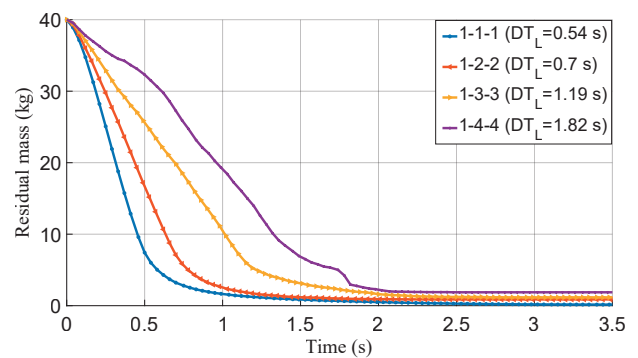
**Fig. 11** Distribution of density in the silo and total bulk density (TBD) in the models of comparison 2: **a)** 1-1-1, **b)** 1-2-2, **c)** 1-3-3, **d)** 1-4-4.



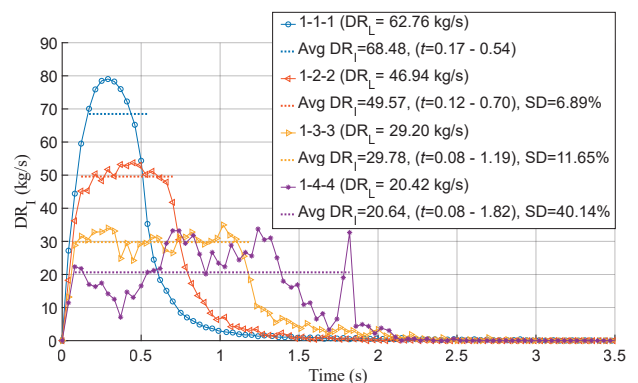
**Fig. 12** Velocity profiles of the considered models obtained during discharge at different heights from the outlet, ranging from 50 mm to 450 mm, and at two instants of time,  $t = 0.1$  s and  $t = 0.2$  s, comparison #2. The raw data are publicly available at J-STAGE Data (<https://doi.org/10.50931/data.kona.28561904>).

Regarding the differences in discharge rates, an increase in particle size using 8, 27, and 64 spheres resulted in 45 %, 64 %, and 86 % lower discharge rates, respectively. The standard deviations of  $DR_L$  also show the different flow presented, with 11.11 %, 23.75 %, and 43.23 %, in models 2-2-2, 3-3-3, and 4-4-4, respectively.

**Fig. 19** shows the total bulk densities of all these models. The values decreased as the particle size increased, regardless of particle shape. However, the largest particles in the 4-4-4 model did not follow the same trend as observed when considering models 2-2-2 and 3-3-3, which could be attributed to the large ratio between silo width and particle size. Additionally, some models with different particle shapes and sizes exhibited similar bulk densities, particularly when comparing 1-2-2 with 1-1-3, 1-2-2 with 1-3-3,



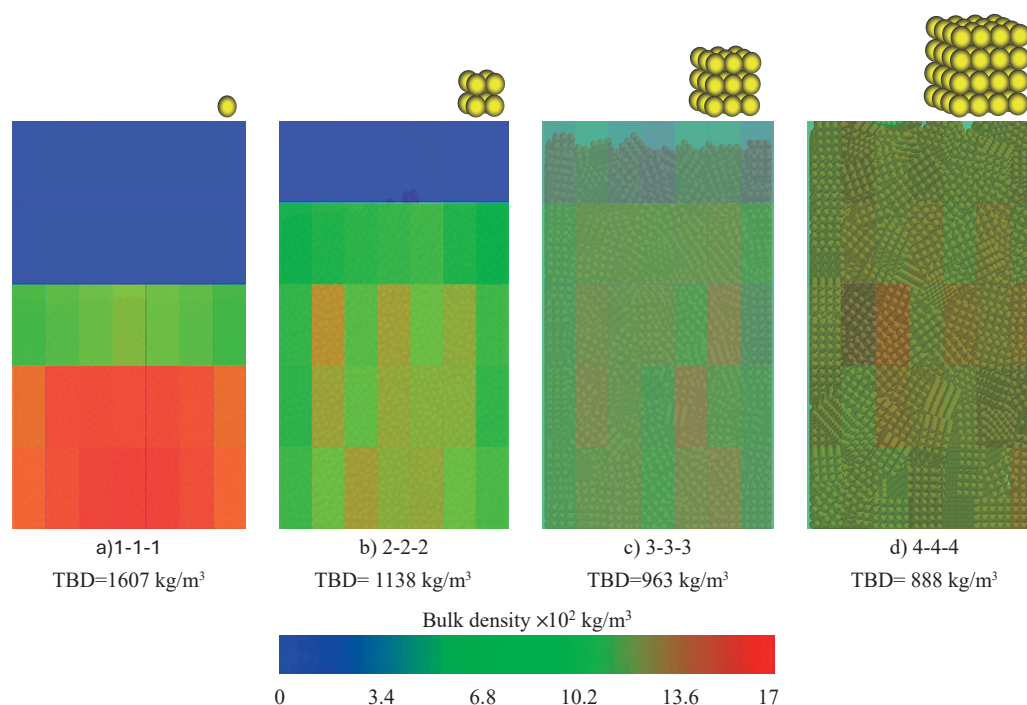
**Fig. 13** Residual mass in the silo (kg) vs. discharge time (s), flatness variation. The raw data are publicly available at J-STAGE Data (<https://doi.org/10.50931/data.kona.28561904>).



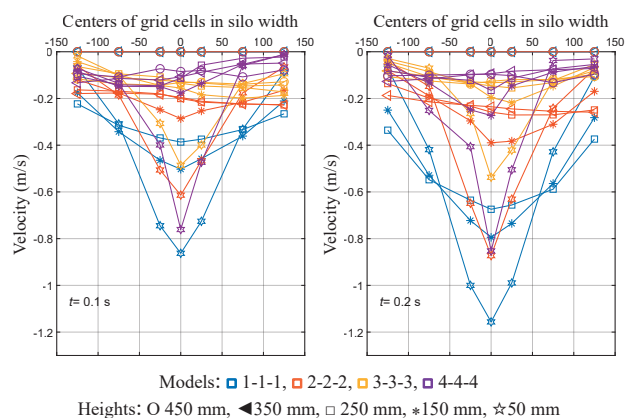
**Fig. 14** Instantaneous discharge rate ( $DR_L$ ) (kg/s) vs. time with 0.04 s time step, average instantaneous discharge rate ( $Avg DR_L$ ) (kg/s), and overall discharge rate values ( $DR_L$ ), flatness variation.

and 3-3-3 with 1-4-4. These similarities in bulk densities were also reflected in the average discharge rates (**Fig. 20**) and the standard deviation of the flow fluctuations

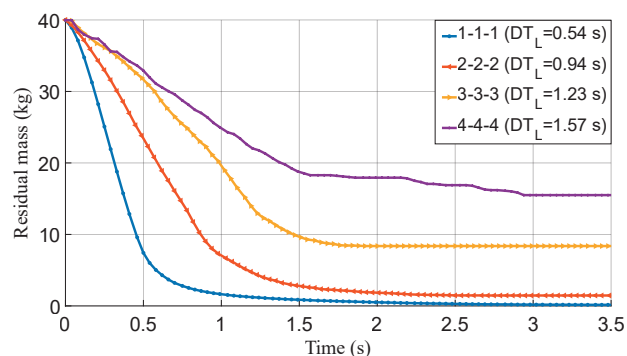




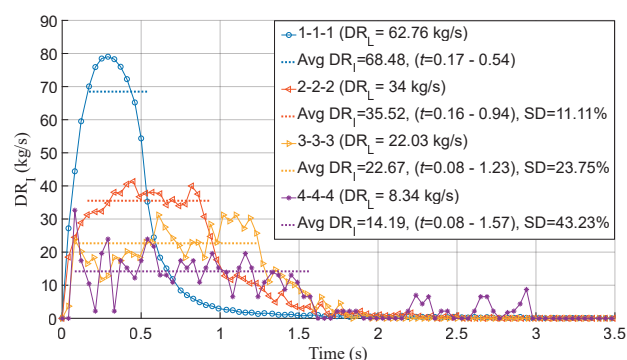
**Fig. 15** Distribution of density in the silo and total bulk density (TBD) in the models of comparison 3: **a)** 1-1-1, **b)** 2-2-2, **c)** 3-3-3, **d)** 4-4-4.



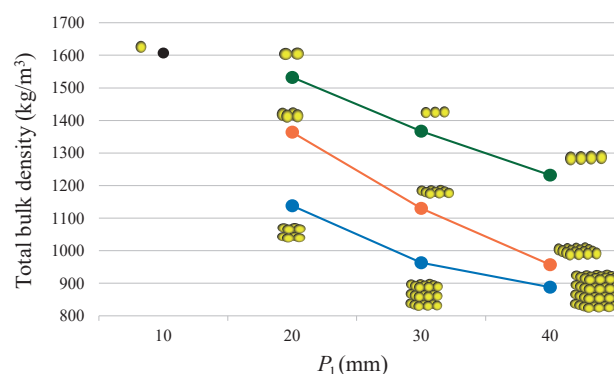
**Fig. 16** Velocity profiles of the considered models obtained during discharge at different heights from the outlet, ranging from 50 mm to 450 mm, and at two instants of time,  $t = 0.1$  s and  $t = 0.2$  s, comparison #3. The raw data are publicly available at J-STAGE Data (<https://doi.org/10.50931/data.kona.28561904>).



**Fig. 17** Residual mass in the silo (kg) vs. discharge time (s), compactness size variation. The raw data are publicly available at J-STAGE Data (<https://doi.org/10.50931/data.kona.28561904>).



**Fig. 18** Instantaneous discharge rate ( $DR_I$ ) (kg/s) vs. time with 0.04 s time step, average instantaneous discharge rate (Avg  $DR_I$ ) (kg/s), and overall discharge rate values ( $DR_L$ ), compactness size variation.



**Fig. 19** Total bulk densities of models varying in size of slender, flat, and compact particles.

(Table 4). Although model 4-4-4 did not align with the bulk density trend observed above, its discharge rate followed the trend observed in models 2-2-2 and 3-3-3

(Fig. 20). Models 1-1-3 and 1-2-2 presented a standard deviation of approximately 7 %, whereas models 1-1-4, 1-3-3, and 2-2-2 had a standard deviation of approximately 11 %. However, models 1-4-4 and 3-3-3 showed significantly different values (40.14 % and 23.75 %, respectively). This indicates a potential relationship between slender, flat, and compact shapes. To confirm this, further models should be developed.

Comparing both the bulk density and the average discharge rate of models with the same ( $P_1$ ): 1-1-2, 1-2-2, and 2-2-2; 1-1-3, 1-3-3, and 3-3-3; and 1-1-4, 1-4-4, and 4-4-4, similar differences were found in the average discharge rates due to the different packing configurations obtained. In order to obtain more information on the effect of the variation of the particle shape from elongated to flat and compact particles on the discharge behavior, three more

comparisons (#4, #5, and #6) were established. The results are analyzed as follows.

### 3.4 Comparison #4

In Comparison 4, the variation in particle shape from slender to compact was analyzed. The models 1-1-1, 2-2-4, 3-3-4, and 4-4-4 were evaluated, each characterized by different aspect ratios ( $P_w/P_1$ ). The total bulk density for models with  $P_w/P_1$  ratios of 0.5, 0.75, and 1 was 17 %, 22 %, and 27 % lower, respectively, than the total bulk density of model 1-1-4 with a ( $P_w/P_1$ ) ratio equal to 0.25 (Fig. 21). As shown in Fig. 21, a substantial decrease in bulk density was observed when  $P_w$  was varied from 1 to 2, representing a 17 % decrease. Subsequent increases in the aspect ratio resulted in more moderate and consistent density decreases of approximately 6.5 % and 6.9 % when ( $P_w$ ) varied from 2 to 3 and from 3 to 4, respectively. Model 4-4-4 exhibited a less uniform bulk density distribution than the others. Larger voids were observed at various locations within the silo, which are indicated by blue or near-blue colors. Fig. 22 displays the velocity profiles with a V-shaped pattern below 250 mm from the outlet, and Fig. 23 shows the residual masses with the  $DT_L$  values for all the models.

As illustrated in Fig. 24, the flow was irregular in all cases. The residual masses obtained (Fig. 23) indicated that clogging might occur in models with larger particles, as evidenced in models 3-3-4. In case that clogging does not occur, the bulk material remains in the silo after discharge, as observed in model 4-4-4. Regarding discharge rates, an increase in ( $P_w$ ) from ( $P_w = 1$ , slender) to ( $P_w = 4$ , compact

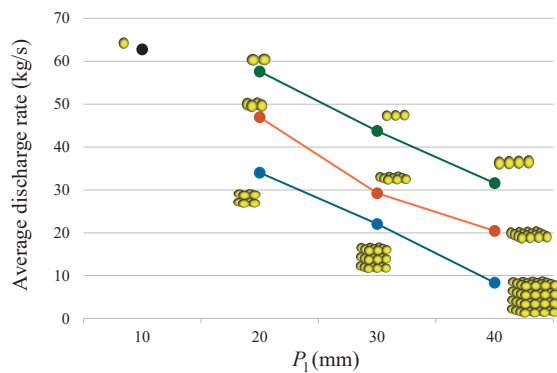


Fig. 20 Average discharge rates of models varying in size of slender, flat, and compact particles.

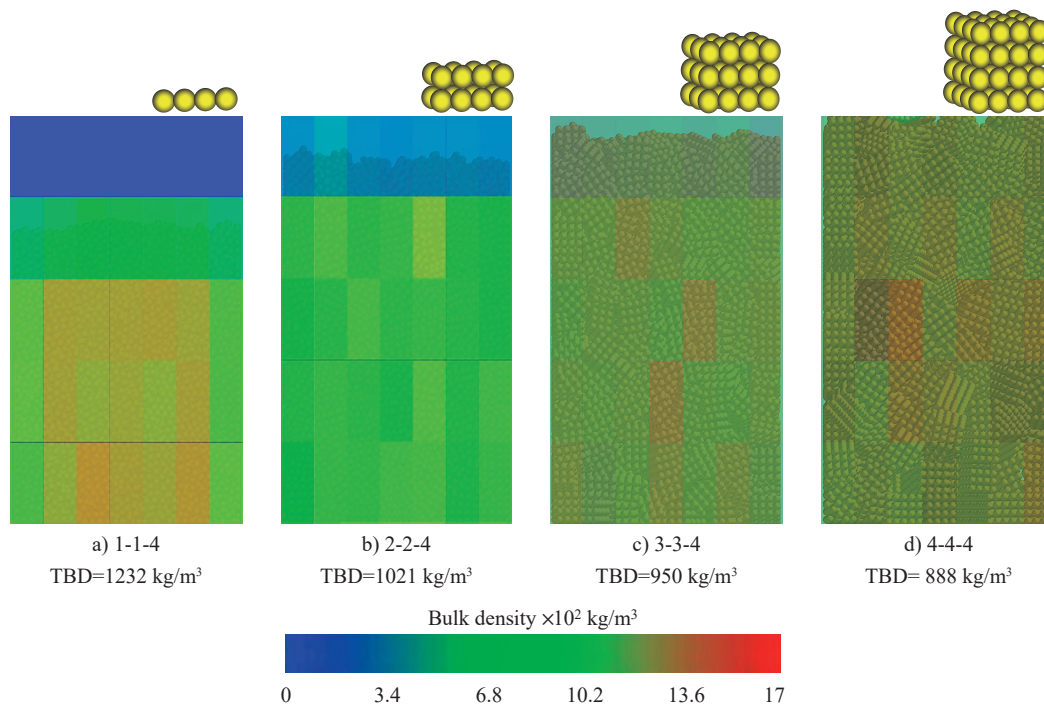
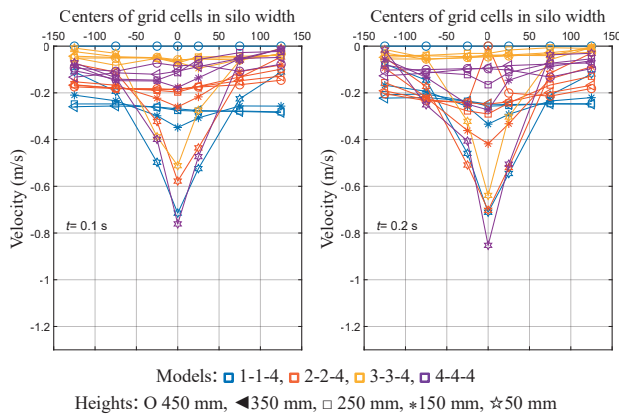
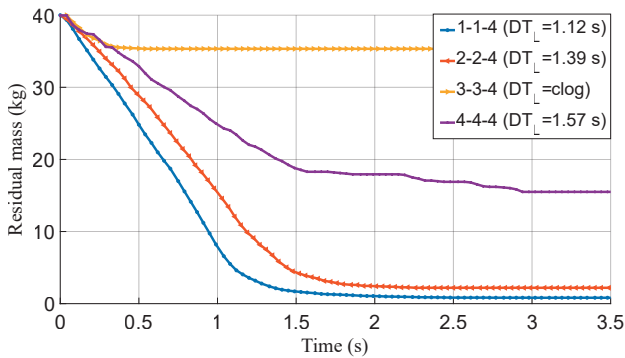


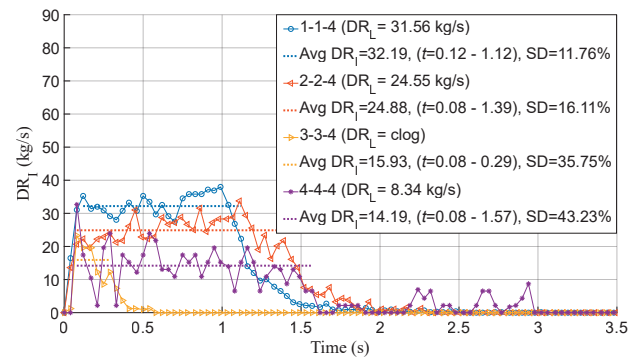
Fig. 21 Distribution of density in the silo and total bulk density (TBD) in the models of comparison 4: a) 1-1-4, b) 2-2-4, c) 3-3-4, d) 4-4-4.



**Fig. 22** Velocity profiles of the considered models obtained during discharge at different heights from the outlet, ranging from 50 mm to 450 mm, and at two instants of time,  $t = 0.1$  s and  $t = 0.2$  s, comparison #4. The raw data are publicly available at J-STAGE Data (<https://doi.org/10.50931/data.kona.28561904>).



**Fig. 23** Residual mass in the silo (kg) vs. discharge time (s), slender to compact variation. The raw data are publicly available at J-STAGE Data (<https://doi.org/10.50931/data.kona.28561904>).

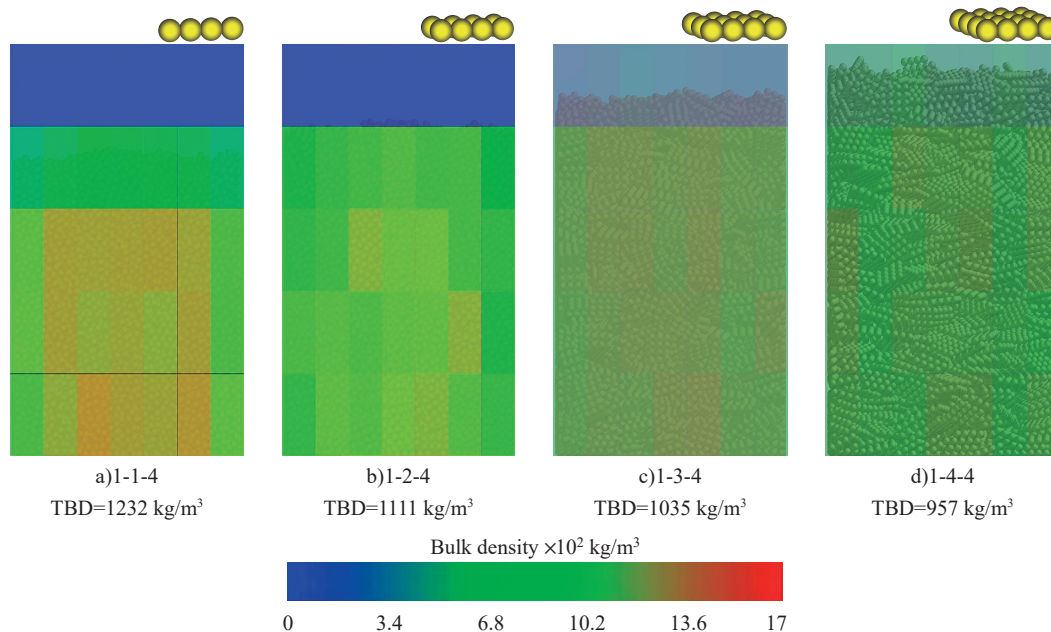


**Fig. 24** Instantaneous discharge rate ( $DR_L$ ) (kg/s) vs. time with 0.04 s time step, average instantaneous discharge rate (Avg  $DR_L$ ) (kg/s), and overall discharge rate values ( $DR_L$ ), slender to compact variation.

shape) with an aspect ratio ( $P_w/P_l$ ) from 0.25 to 1 resulted in values ranging from 31.56 to 8.34, respectively, and regarding the SD of the  $DR_L$  from 11.76 % to 43.23 %.

### 3.5 Comparison #5

In Comparison 5, the variation in particle shape from elongated to flat was analyzed. The models 1-1-4, 1-2-4, 1-3-4, and 1-4-4 were considered, each with different ratios ( $P_h/P_w$  and  $P_w/P_l$ ). The total bulk density for models with aspect ratios ( $P_h/P_w$ ) of 0.5, 0.33, and 0.25 was 9 %, 15 %, and 22 % lower, respectively, than the total bulk density of model 1-1-4 with ( $P_h/P_w$ ) equal to one (Fig. 25). The bulk density was more evenly distributed in model 1-4-4 than in the other models, although it was still less uniform than in model 4-4-4 from comparison #4. Fig. 26 shows the velocity profiles with a V-shape below 250 mm from the outlet. A similar behavior was observed during discharge in models 1-2-4 and 1-3-4. However, the behavior of model

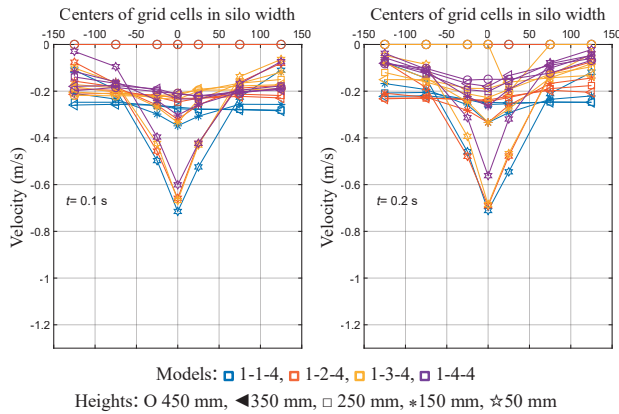


**Fig. 25** Distribution of density in the silo and total bulk density (TBD) in the models of comparison 5: a) 1-1-4, b) 1-2-4, c) 1-3-4, d) 1-4-4.

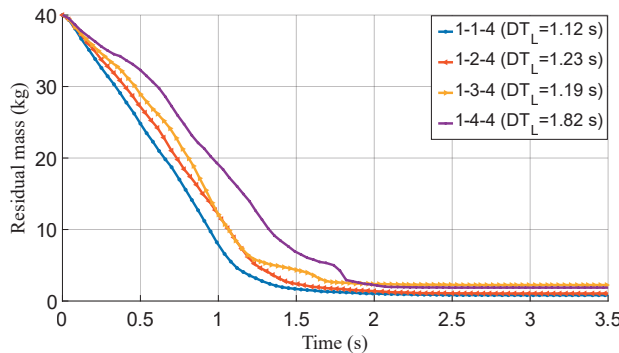


1-4-4 differed from that of the other three models. This trend is also observed in Figs. 27 and 28, where the residual mass, discharge time, and instantaneous discharge rate are presented.

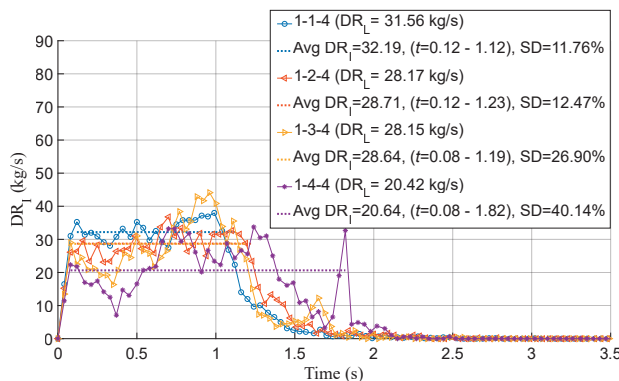
Regarding discharge rates, an increase of the aspect ratio ( $P_h/P_w$ ) from 0.25 ( $P_w = 4$ ) to 1 ( $P_w = 1$ ) resulted in an in-



**Fig. 26** Velocity profiles of the considered models obtained during discharge at different heights from the outlet, ranging from 50 mm to 450 mm, and at two instants of time,  $t = 0.1$  s and  $t = 0.2$  s, comparison #5. The raw data are publicly available at J-STAGE Data (<https://doi.org/10.50931/data.kona.28561904>).



**Fig. 27** Residual mass in the silo (kg) vs. discharge time (s), slender to flat variation. The raw data are publicly available at J-STAGE Data (<https://doi.org/10.50931/data.kona.28561904>).



**Fig. 28** Instantaneous discharge rate ( $DR_L$ ) (kg/s) vs. time with 0.04 s time step, average instantaneous discharge rate (kg/s) (Avg  $DR_L$ ), and overall discharge rate values ( $DR_L$ ), slender to flat variation.

crease in charge rate from 20.42 to 31.56 kg/s, and a decrease in the standard deviation of  $DR_L$  from 40.14 % to 11.76 %, respectively. The largest particles, both flat and compact, exhibited the highest fluctuations around 40 %.

### 3.6 Comparison #6

In Comparison 6, the variation in particle shape from flat to compact was analyzed. The particle shape was varied by altering the aspect ratio ( $P_h/P_w$ ) while keeping the width ( $P_w = 4$ ) and particle length ( $P_l = 4$ ) constant. In this comparison, models 1-4-4, 2-4-4, 3-4-4, and 4-4-4 were analyzed with different particle shapes and degrees of flatness. Fig. 29 plots the bulk density for all models as the ( $P_h$ ) value varied. The density was evenly distributed across all four models, with the most significant differences observed for model 4-4-4.

The total bulk density for models with aspect ratios ( $P_h/P_w$ ) of 0.5, 0.75, and 1 varied with differences of 0.2 % higher and 5 % and 7 % lower, respectively, compared to the total bulk density of model 1-4-4 with ( $P_h/P_w$ ) equal to 0.25.

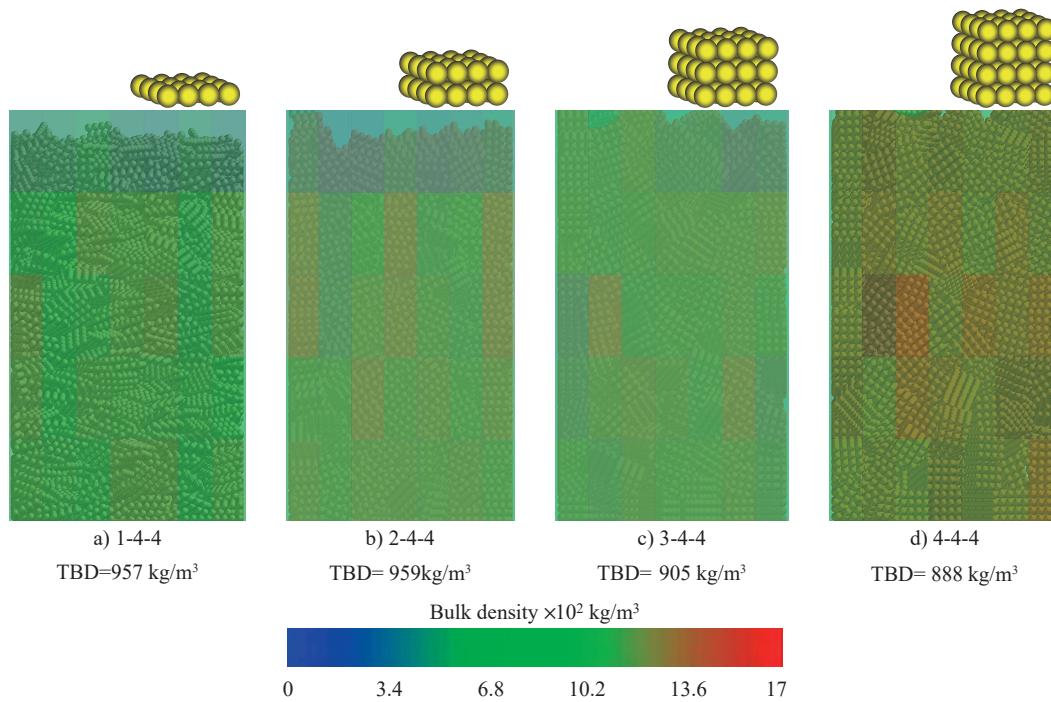
In Fig. 30, the velocity profiles exhibited a V-shaped pattern below 150 mm from the outlet. A comparison of velocities at 50 mm height at 0.1 s revealed values of 0.60, 0.59, 0.47, and 0.76 m/s for the respective models. At 0.2 s, the velocities were 0.56, 0.26, 0.28, and 0.85 m/s. These velocity profiles indicate an unsteady flow with particles discharging faster near the outlet and slower further above it, particularly at a height of 150 mm. The higher residual mass values indicate that geometric interlocking effects are more pronounced above this height when dealing with compact particle shapes than in other cases.

Figs. 31 and 32, which display the residual mass and instantaneous discharge rate, highlight the differences in discharge indicators, such as  $DR_L$  and  $DT_L$ . The models 2-4-4, 3-4-4, and 4-4-4 showed similar Avg  $DR_L$  and SD values, so they could be grouped as showing a similar behavior during discharge, although in the residual mass they exhibited some differences. This evidence reveals the influence of this type of shape (compact) on the flow behavior.

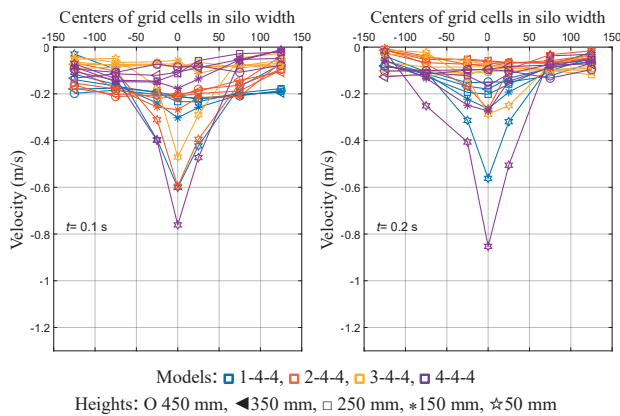
Figs. 33 and 34 show the total bulk density and average discharge, respectively, of the models with spherical, slender, flat, and compact particles. The total bulk density tended to decrease with increasing particle size and compactness. Fig. 33 shows that the variation in bulk density is lower when the particle is compact. The cubic geometry seems to help with the accommodation of the particles during filling compared with slender and flat particles. Regarding the discharge rate in Fig. 34, the largest difference was observed for the slender particles, which may have been facilitated by their geometry toward the outlet.

When comparing all scenarios, larger particles with higher elongation, flatness, and compactness tend to form less dense packing structures, leading to lower bulk

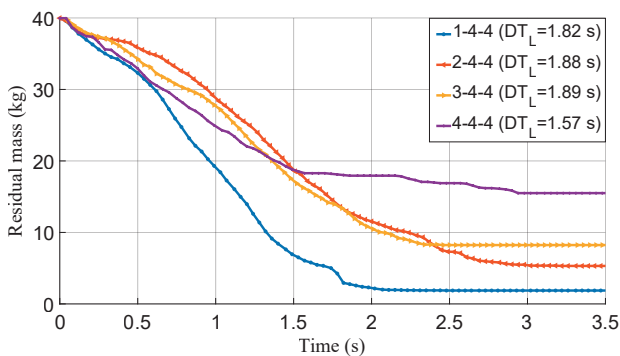




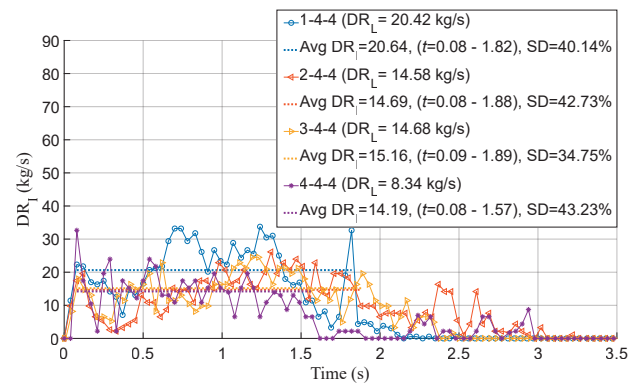
**Fig. 29** Distribution of density in the silo and total bulk density (TBD) in the models of comparison 6: **a)** 1-4-4, **b)** 2-4-4, **c)** 3-4-4, **d)** 4-4-4.



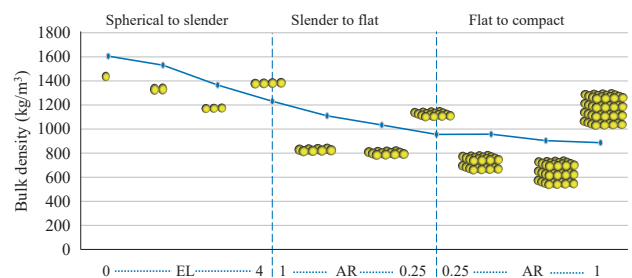
**Fig. 30** Velocity profiles of the considered models obtained during discharge at different heights from the outlet, ranging from 50 mm to 450 mm, and at two instants of time  $t = 0.1$  s and  $t = 0.2$  s, comparison #6. The raw data are publicly available at J-STAGE Data (<https://doi.org/10.50931/data.kona.28561904>).



**Fig. 31** Residual mass in the silo (kg) vs. discharge time (s), flat to compact variation. The raw data are publicly available at J-STAGE Data (<https://doi.org/10.50931/data.kona.28561904>).



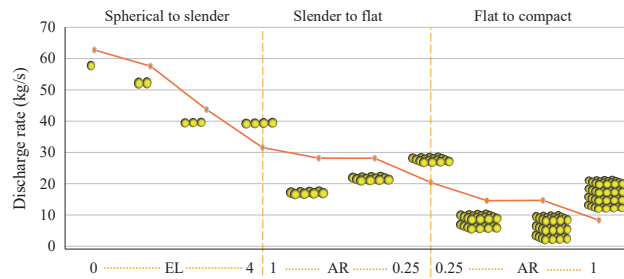
**Fig. 32** Instantaneous discharge rate ( $DR_L$ ) (kg/s) vs. time with 0.04 s time step, average instantaneous discharge rate (Avg  $DR_L$ ) (kg/s), and overall discharge rate values ( $DR_L$ ), flat to compact variation.



**Fig. 33** Total bulk densities of the models varying from spherical to slender particles, slender to flat particles, and flat to compact particles.

densities. The effect of shape variation differed in each comparison, depending on the specific values of aspect ratios.

In all models, a classical V-shaped velocity profile was



**Fig. 34** Discharge rates ( $DR_i$ ) of models varying from spherical to slender particles, slender to flat particles, and flat to compact particles.

observed. This indicates that the particle velocities are higher near the center and lower toward the silo walls. At 0.1 and 0.2 s, particles with lower aspect ratios, lower elongation, and smaller sizes exhibited higher velocities. Stagnant zones were observed during discharge, with particles near the silo walls remaining stationary. This trend was particularly evident in elongated, flat particles with higher aspect ratios and compact particles with larger sizes. The analysis of residual masses, discharge rates, and discharge times provided insights into the dynamics of the silo discharge process for different particle shapes. As expected, the discharge rate was influenced by the size, elongation, and aspect ratio of the particles, with large particles resulting in erratic flows. The particle interlocking was noted to increase the discharge time and affect the flow smoothness.

Different methods were used to determine the particle size, which provided different  $K/P$  ratios (Table 4), leading to various recommendations for transitioning from smooth to irregular flow. The threshold values were as follows:  $K/P \approx 10$  when using  $P_{eq}$ ,  $K/P \approx 7$  when using  $P_l$ , and  $K/P \approx 6$  when using  $P_{d(2D)}$  or  $P_{d(3D)}$ . Values below these thresholds correspond to irregular flows in all models. Considering the aforementioned methods, the use of the equivalent diameter ( $P_{eq}$ ) has the drawback of not accounting for particle shape. This is evident in models 1-4-4 and 2-2-4 (Table 4), where despite the same  $K/P_{eq}$  ratio (5.95), two different discharge flows with standard deviations of 40.14 and 16.11 %, respectively, were observed. Concerning the use of  $P_l$ , Table 4 shows that some particle shape configurations yield the same  $K/P$  ratio, such as those in comparisons #4, #5, and #6, which all show a  $K/P$  ratio of 3.75 and different discharge flows. The standard deviation of the instantaneous discharge rate in these models varied from 11.76 % to 43.23 %, indicating that the use of this dimension to estimate the particle size is not suitable for differentiating irregular flows. A similar conclusion was drawn for  $P_{d(2D)}$ . Identical values of  $K/P_{d(2D)}$  were found in comparison #2 (flat particles) and #3 (compact particles) for different particle shape configurations. In addition, in comparison #6 (flat to compact), all models had the same  $K/P_{d(2D)} = 2.88$ . However, in this case, the models pre-

sented standard deviations of the instantaneous discharge rate, ranging from 34.75 % to 43.23 %, indicating different discharge flows. To distinguish non-smooth flows,  $P_{d(3D)}$  is more suitable. The obtained values for  $K/P_{d(3D)}$  in the compared models improve the differentiation of the flow type, allowing for the establishment of a potential classification according to the standard deviation of the instantaneous discharge rate. When the  $K/P_{d(3D)}$  value is less than three, the flow fluctuations exhibit a standard deviation of approximately 40 %, which can be considered as a threshold for identifying excessive irregular flows.

Given these observations, careful consideration is necessary when determining particle size for the  $K/P$  ratio as an indicator of flow type during the discharge of complex particle shapes in a silo.

#### 4. Conclusions

This research investigated the  $K/P$  ratio and the effect of particle shape variation on the flow behavior in a flat-bottom silo with slot opening using the discrete element method. Sixteen different models were developed, covering different elongation and aspect ratio variations. A total of 40 kg of particles was considered for each model. The models ranged from 10 mm diameter spherical particles to compact particle shapes generated using clusters of spheres.

The analysis of the results revealed information on the bulk densities developed during the filling process in each model and on the distribution of the velocity profiles at 0.1 and 0.2 s after the opening of the outlet. Also, residual masses and average discharge rates were analyzed, revealing the percentage variations within each model. The results demonstrate the significant influence of particle size and shape on the discharge process in a flat-bottom silo.

Therefore, caution is advised when interpreting the results of the DEM simulations of bulk materials with simplified particle shapes. At least essential shape factors, such as the elongation or aspect ratio of the real particle, should be considered in the representation of the simplified particle shape used in numerical models. The  $K/P$  ratio can be used to indicate the type of flow generated inside the silo. The value for parameter  $P$  should consider the maximum length of the particle ( $P_{d(3D)}$ ), especially for flat and compact particle shapes, since others, such as  $P_{eq}$ ,  $P_l$ , or  $P_{d(2D)}$ , have been shown to be not suitable for slender, flat, and compact particles.

A value of about six was identified as the threshold for differentiating the type of flow for these particle shape configurations. Getting lower  $K/P$  values would indicate that fluctuations and an intermittent discharge rate would be present, while values significantly higher would indicate that a sudden discharge would be produced, showing lower discharge times.

## Nomenclature

AR	aspect ratio
$DR_L$	average discharge rate in the linear curve ( $\text{kg s}^{-1}$ )
$DR_I$	instantaneous discharge rate ( $\text{kg s}^{-1}$ )
$DT_L$	discharge time of the linear curve (s)
EL	elongation
$H$	silo height (mm)
$K/P$	slot width to particle size ratio
$K$	slot width (mm)
$P_{d(3D)}$	max orthogonal length of the particles (mm)
$P_{d(2D)}$	maximum Feret length of the 2D projection (mm)
$P_{eq}$	diameter length at the equivalent volume of a sphere (mm)
$P_h$	the third particle length (mm)
$P_l$	max normal length of particles (mm)
$P_w$	the second longest particle length (mm)
SD	standard deviation
TBD	total bulk density ( $\text{kg m}^{-3}$ )
$W$	silo width
$\rho_b$	bulk density ( $\text{kg m}^{-3}$ )
*	reference model

## Data Availability Statement

The data from the numerical investigation of the discharge behavior in a flat-bottom silo (depicted in **Figs. 8–9, 12–13, 16–17, 22–23, 26–27, 30–31**) are available publicly in J-STAGE Data (<https://doi.org/10.50931/data.kona.28561904>).

## References

- Alonso-Marroquín F., Ramírez-Gómez Á., González-Montellano C., Balaam N., Hanaor D.A.H., Flores-Johnson E.A., Gan Y., Chen S., Shen L., Experimental and numerical determination of mechanical properties of polygonal wood particles and their flow analysis in silos, *Granular Matter*, 15 (2013) 811–826. <https://doi.org/10.1007/s10035-013-0443-7>
- Bharadwaj R., Ketterhagen W.R., Hancock B.C., Discrete element simulation study of a Freeman powder rheometer, *Chemical Engineering Science*, 65 (2010) 5747–5756. <https://doi.org/10.1016/j.ces.2010.04.002>
- Brown R.L., Richards J.C., Kinematics of the flow of dry powders and bulk solids, *Rheologica Acta*, 4 (1965) 153–165. <https://doi.org/10.1007/BF01969251>
- Cundall P.A., Strack O.D.L., A discrete numerical model for granular assemblies, *Géotechnique*, 29 (1979) 47–65. <https://doi.org/10.1680/geot.1979.29.1.47>
- EDEM 2022.3, User Guide, Edinburgh, Scotland, UK: DEM Solutions, Ltd., 2023. [https://2022.help.altair.com/2022.3/EDEM/Introducing\\_EDEM.htm](https://2022.help.altair.com/2022.3/EDEM/Introducing_EDEM.htm)
- Favier J.F., Abbaspour-Fard M.H., Kremer M., Raji A.O., Shape representation of axis-symmetrical non-spherical particles in discrete element simulation using multi-element model particles, *Engineering Computations*, 16 (1999) 467–480. <https://doi.org/10.1108/02644409910271894>
- González-Montellano C., Gallego E., Ramírez-Gómez Á., Ayuga F., Three dimensional discrete element models for simulating the filling and emptying of silos: Analysis of numerical results, *Computers & Chemical Engineering*, 40 (2012) 22–32. <https://doi.org/10.1016/j.compchemeng.2012.02.007>
- Gelnar D., Zegzulka J., *Discrete Element Method in the Design of Transport Systems: Verification and Validation of 3D Models*, Springer International Publishing, Cham, 2019, ISBN: 978-3-030-05712-1. <https://doi.org/10.1007/978-3-030-05713-8>
- Horabik J., Parafiniuk P., Więcek J., Kobylka R., Molenda M., Stasiak M., DEM modelling of the influence of initial stress state on the discharge rate of spherical particles from a model silo, *Powder Technology*, 403 (2022) 117402. <https://doi.org/10.1016/j.powtec.2022.117402>
- Langmaid R.N., Rose H.E., Arch formation in a non-cohesive granular material, *Journal of Institute of Fuel*, 30 (1957) 166–172.
- Nedderman R.M., Tüzün U., Savage S.B., Houlisby G.T., The flow of granular materials—I: Discharge rates from hoppers, *Chemical Engineering Science*, 37 (1982) 1597–1609. [https://doi.org/10.1016/0009-2509\(82\)80029-8](https://doi.org/10.1016/0009-2509(82)80029-8)
- Radvilaitė U., Ramírez-Gómez Á., Kačianauskas R., Determining the shape of agricultural materials using spherical harmonics, *Computers and Electronics in Agriculture*, 128 (2016) 160–171. <https://doi.org/10.1016/j.compag.2016.09.003>
- Ramírez A., Nielsen J., Ayuga F., On the use of plate-type normal pressure cells in silos: part 2: validation for pressure measurements, *Computers and Electronics in Agriculture*, 71 (2010) 64–70. <https://doi.org/10.1016/j.compag.2009.12.005>
- Ramírez-Gómez Á., The discrete element method in silo/bin research. Recent advances and future trends, *Particulate Science and Technology*, 38 (2020) 210–227. <https://doi.org/10.1080/02726351.2018.1536093>
- Žurovec D., Hlosta J., Nečas J., Zegzulka J., Monitoring bulk material pressure on bottom of storage using DEM, *Open Engineering*, 9 (2019) 623–630. <https://doi.org/10.1515/eng-2019-0080>

## Authors' Short Biographies



**Yani Alhaddad** is a Ph.D. student in Production Engineering and Industrial Design at Universidad Politécnica de Madrid. He has completed advanced studies with a master's degree in mechanical engineering modeling from Budapest University of Technology and Economics. He holds a bachelor's degree in mechanical engineering from Hashemite University. His research interests focus on machine design, product development, modeling and simulation, computer-aided design, and discrete element method (DEM).



**Prof. Dr. Álvaro Ramírez-Gómez** is a Full Professor of Industrial Design Engineering at the Escuela Técnica Superior de Ingeniería y Diseño Industrial-Universidad Politécnica de Madrid (UPM). Prior to entering Academia, he was in professional practice as a Project Engineer. He completed his Ph.D., obtaining the mention of “European Doctor” at UPM. Hitherto, he has accumulated experience as a research explorer through 16 visits to universities and research centers, such as Aalborg University-SBi, The University of Edinburgh, The University of Sydney, Melbourne University, and Vilnius Gediminas Technical University. He has published over 60 scientific articles and editorials in indexed journals (Scopus h-index: 25).